International Journal of Fracture **101:** 141–159, 2000.

Failure mode transition in ceramics under dynamic multiaxial compression

W. CHEN[1] and G. RAVICHANDRAN[2]
[1]*Department of Aerospace and Mechanical Engineering, The University of Arizona, Tucson, AZ 85721, U.S.A.*
e-mail: wchen@allen.ame.arizona.edu
[2]*Graduate Aeronautical Laboratories, California Institute of Technology, Pasadena, CA 91125, U.S.A.*

Received 28 April 1999; accepted in revised form 25 June 1999

Abstract. An experimental technique based on the Kolsky pressure bar has been developed to investigate the behavior of ceramics under dynamic multiaxial compression. Experimental results for aluminum nitride (AlN), together with data available in the literature, indicate that a Mohr-Coulomb criterion and the Johnson–Holmquist model fit the experimental data for failure in a brittle manner, whereas the ceramic material exhibited pressure insensitive plastic flow at high pressures. A failure surface is constructed which represents the material failure behavior, including brittle failure, brittle/ductile transition and plastic flow, under various pressures. The effect of various material properties on the failure behavior was investigated. The Poisson's ratio is found to be a measure of brittleness for ceramic materials with low spall strength under shock wave loading conditions. Lower value of Poisson's ratio indicates that the material will fail in a brittle manner through axial splitting even under uniaxial strain loading; whereas materials with higher Poisson's ratio may be expected to deform plastically beyond the Hugoniot Elastic Limit (HEL). The applicability of the proposed failure surface to a range of ceramics is explored and the limitations of the model are outlined.

Key words: Ceramics, dynamic fracture, brittle/ductile transition, failure surface, aluminum nitride, multiaxial compression.

1. Introduction

Ceramics and ceramic composites are being used increasingly as structural materials in a variety of applications subjected to dynamic loading. Due to rapid advances in processing technology, high strength ceramics and ceramic composites are being developed with exceptional mechanical properties. Since relatively little is known about the mechanical behavior of ceramic materials in comparison to metallic structural materials, monolithic ceramics and ceramic composites have been at the forefront of advanced materials research. In order to accurately model dynamically loaded ceramic structures and to efficiently use ceramic materials in various structural applications, it is essential to establish proper failure criteria for these materials. Experimental investigations into the failure behavior of ceramic materials have been conducted under quasi-static uniaxial and multiaxial loading conditions. For example, Heard and Cline (1980) studied the mechanical behavior of various types of polycrystalline BeO, Al_2O_3, and AlN ceramics under quasi-static loading at confining pressures up to 1.25 GPa using a tri-axial testing facility. Dynamic experimental data available in the literature essentially were limited to the results from two specific loading paths: uniaxial stress (1-D stress) and uniaxial strain (1-D strain). Typically, the uniaxial stress experiments are performed using the Kolsky (split Hopkinson) pressure bar, whereas the uniaxial strain experiments are conducted using plate impact techniques. Plate impact experiments have produced a considerable

amount of data on the Hugoniot elastic limit (HEL) and spall strength of ceramics (Grady, 1998).

Recently, in order to better understand the effects of loading conditions on failure behavior of ceramics, experimental investigations have been performed on the dynamic failure behavior of ceramic materials under multiaxial compression (Lankford, 1994; Chen and Ravichandran, 1996b, 1997). Proper modeling of the mechanical behavior of ceramic materials under dynamic loading conditions has also been attempted. For example, Rajendran (1994) developed constitutive models for ceramic materials using a damage mechanics approach with a scalar damage parameter and used the models in the numerical simulations of the response of a ceramic/metal structure under impact loading conditions. Johnson and Holmquist (1994) proposed a computational constitutive model for brittle materials subject to large strains, high strain rates and high pressure, known as JH-2 model, which was found to fit the failure behavior of ceramics in the brittle failure region as discussed later. Grady (1998) attempted to use the variation of the ratio of spall strength to HEL as a function of the Poisson's ratio for various ceramics to fit the failure models proposed by Murrel (1963) and Rosenberg (1993). However, these models were either restricted to specific applications or did not fit experimental data. There has been little success in explaining the trends associated with the dynamic behavior or performance of ceramic materials.

In this paper, a failure surface on Mohr–Coulomb plane for ceramic materials is proposed based on theoretical arguments and experimental evidence. The compressive strength data collected from experiments under dynamic multi-axial compression, although limited in quantity, provide experimental evidence on the failure behavior of ceramics under varying loading paths. These data depict a more complete background from which a more realistic failure criterion for ceramics may be established such as the failure surface proposed in this paper. The proposed failure surface provides clues toward resolving some existing controversies about performance of ceramic materials under dynamic loading. The possible mechanisms for plastic flow beyond HEL in materials under high pressure are outlined and are examined in the light of available experimental data.

2. Experimental

2.1. Modified kolsky (split hopkinson) bar

The dynamic axial loading device is a modified Kolsky (split Hopkinson) pressure bar with a single loading capability. The cylindrical specimen is confined laterally by a shrink fit metal sleeve. In this section, the modified Kolsky pressure bar is briefly described. The details of this technique can be found elsewhere (Chen and Ravichandran, 1996a, 1997).

Kolsky (split Hopkinson) pressure bar is a well-established apparatus commonly utilized in the high-strain-rate testing of materials; see Follansbee (1985). Originally developed by Kolsky (1949), the concept has found widespread applications in testing ductile materials at strain rates up to $10^4\ \mathrm{s}^{-1}$. This technique has been directly applied without any modification to brittle ceramics and ceramic composite materials in dynamic uniaxial compression experiments; see, for example, Lankford (1977). However, when brittle materials such as ceramics and ceramic composites are tested in the conventional Kolsky pressure bar, the limitations of the technique must be recognized. In order to obtain reliable and consistent experimental data when testing these materials with the Kolsky bar, appropriate modifications must be incorporated in both the experimental technique and the design of specimen geometry. Many modifications to the

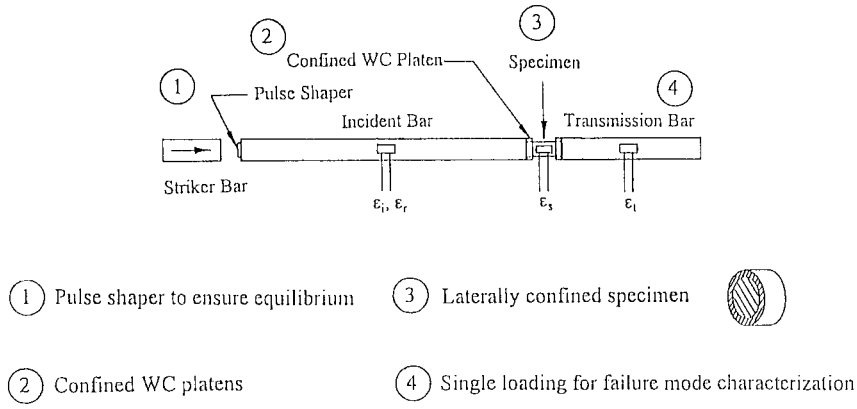

Figure 1. Schematic of a modified Kolsky (split Hopkinson) pressure bar for investigating ceramics under multiaxial compression.

Kolsky pressure bar technique and the specimen design have been proposed in the recent literature. A schematic of a modified Kolsky pressure bar is shown in Figure 1.

The principal modifications of the conventional Kolsky bar technique to study hard and brittle materials such as ceramics include,

(i) *Pulse shaping*: shaping of the loading pulse by a thin copper disc, called a pulse shaper, placed at the impact end of the incident bar has been used to prevent the ceramic specimen from failing before equilibrium is attained. Based on an analysis of one-dimensional elastic wave propagation between the specimen and the elastic bars in Kolsky pressure bar apparatus, Ravichandran and Subhash (1994) established the limiting strain rates that can be attained in a ceramic specimen using the Kolsky pressure bar technique. An incident pulse generated without a pulse shaper will deform the ceramic specimen at strain rates beyond the established limits.

(ii) *Hard platens*: The Kolsky pressure bar has traditionally been used to investigate the plastic behavior of metals that are typically softer than the bar material. Under these conditions, the end surfaces of the bars in contact with the specimen remain flat and parallel during the deformation, which results in a nearly uniform stress state in the specimen. However, when a ceramic material is tested, the harder specimen will indent into the end surfaces of the bars during loading, thus causing stress concentrations at the specimen edges. These stress concentrations will result in the premature failure of the specimen and thus make the experimental data invalid, see Chen et al. (1994). To minimize the problems of indentation and stress concentration, acoustic impedance matched hard and high strength platens need to be placed between the specimen and the bars to prevent indentation and minimize the stress concentrations in the specimen.

(iii) *Direct strain measurement*: Since the strains that are usually accrued during deformation of ceramics are small (1–2 percent), the reflected pulse from Kolsky bar is not capable of providing accurate strain measurement. Reliable strain data has been obtained during testing by mounting strain gauges on the ceramic specimen surface. Both axial and transverse strains can be measured using this technique.

(iv) *Specimen recovery*: Using the conventional Kolsky pressure technique, it is possible for the specimen to be loaded multiple times due to subsequent wave reflections in the incident bar. In order to characterize the failure mode after a well-controlled loading history,

repeated loading of the specimen is undesirable. Single pulse loading can be attained by making the transmission bar shorter than the incident bar. With this modification, the shorter transmission bar will act as a momentum trap, thereby moving the transmission bar away from the specimen before a second compressive loading pulse due to reflected tensile pulse in the incident bar reaches the specimen.

2.2. LATERAL CONFINEMENT

Confinement of the specimen was achieved by installing a shrink fit metal sleeve on the lateral surface of the cylindrical ceramic specimen (Chen and Ravichandran, 1996a, 1997). The inner diameter of the sleeve was slightly smaller than the specimen diameter. To install the sleeve around the specimen, the sleeve was heated to expand the inner diameter and enable the specimen to slide into the sleeve. After the assembly was cooled, shrinkage of the sleeve provided confinement pressure on the lateral surface of the specimen. The magnitude of the confining pressure can be varied by using different materials and thickness for the sleeves. The yield strengths of the sleeve materials were experimentally measured using sleeves which had been subjected to the same thermal cycle as for the specimen-containing sleeves, in order to eliminate any uncertainties due to changes in material properties associated with the thermal cycling. In the case of thin walled sleeves when the sleeve thickness (t) is much smaller than the specimen radius (r), the lateral confinement σ_t can be approximated by

$$\sigma_t \approx \frac{\sigma_y t}{r}, \tag{1}$$

where σ_y is the yield stress of the sleeve material. For a thick walled sleeve, the lateral confinement stress can be computed using the formula given by Chen and Ravichandran (1996a, 1997).

The mechanical confinement technique is advantageous since the sleeves are easy to fabricate and no further modifications to the Kolsky pressure bar are required. Also, the plastically deformed sleeve retains the tested specimen allowing examination of the failure mode, even though the brittle specimen itself may have fragmented during the loading. In computing the stress in the specimen, the contribution from the confining metal sleeve is negated.

2.3. MATERIALS AND EXPERIMENTAL FACILITY

The material used for investigation was a sintered aluminum nitride (AlN) provided by the Dow Chemical Company, Midland, Michigan. The specimens were core-drilled from a quarter inch thick AlN plate, and then ground to the specified dimensions and tolerances. The mechanical properties of sintered aluminum nitride as provided by the manufacturer are listed in Table 1. The specimens were typically 4.76 mm in diameter and 5.48 mm in length. The AlN specimens were ground to be cylindrical within 0.0025 mm on the lateral surface with the two end faces parallel to within 0.0025 mm.

The experiments were conducted in a modified Kolsky pressure bar facility in the Graduate Aeronautical Laboratories at Caltech. The dimensions of the bars used in this study are 1220 and 580 mm in length for the incident and transmission bar respectively, with a common diameter of 19 mm. The striker bars of 19 mm diameter varied in their lengths from 12.5 to 100 mm to achieve the desired loading pulse duration. All the bars were made of high strength Vascomax (C-350) maraging steel (Rockwell hardness, Rc $= 55 - 60$). The yield

Table 1. Physical properties of sintered aluminum nitride (A1N)

Mass Density, ρ	3200 kg/m^3
Young's Modulus, E	307-319 GPa
Poisson's Ratio, ν	0.237
Quasi-static Unconfined Compressive Strength, σ_o	2.5 GPa*

*Measured in this study.

strength of the bars is approximately 2.7 GPa. A pulse shaper that was placed at the impact end of the incident bar was a thin, half hardened copper disc of 0.85 mm in thickness. The diameter and thickness of the copper disc was varied to control the rise time of the incident pulse. Quasi-static experiments were conducted using an MTS servo-hydraulic material testing system.

In order to investigate the influence of confining pressure on dynamic impact strength of the ceramic specimen, four different sleeve materials (copper, brass, high carbon tool steel, and 303 stainless steel) were used in this study. The sleeves were the same length as the specimens, with an outer diameter of 8.17 mm. The inner diameter of the sleeves was typically 0.025 mm less than the specimen diameter. The copper and brass sleeves were heated to 450°C, whereas the steel sleeves were heated to 850 °C for approximately 40 seconds prior to assembly with the specimens. After the sleeve was installed on the specimen, the end faces of the assembly were polished to a 1 μm finish to remove surface damage from the grinding and sleeve installation processes. On each specimen/sleeve assembly, an axial strain gage was mounted on the outer surface of the sleeve to measure the axial strain as a function of time during axial loading. In dynamic experiments, the strain gage signals from incident bar, transmission bar, and the specimen were recorded using a high-speed digital oscilloscope.

2.4. Experimental results

Figure 2 shows the typical quasi-static and dynamic stress-strain curves for sintered AlN specimens with and without confinement. Under both quasi-static and dynamic loading conditions, the unconfined specimens deformed and failed in a typical brittle manner as demonstrated by the nearly linear stress-strain behavior. Upon reaching the maximum (compressive strength) the specimen failed catastrophically as indicated by the sudden drop in stress carrying ability. The stress-strain curve for a confined specimen may be divided into stable and unstable regions. The response of the confined specimens was nearly linear until the peak stress. Under both quasi-static and dynamic loading conditions, the experimental results showed that the failure mode changed from fragmentation by axial splitting without confinement to localized faulting under moderate lateral confinement (120–230 MPa).

Figure 3 shows the compressive strength as a function of lateral confining pressure at two different strain rates. Examination of Figure 3 indicates that the compressive strength increased under both quasi-static and dynamic loading conditions as the lateral confining pressure was increased. The average quasi-static compressive strength of this sintered AlN without confinement is 2.5 GPa, whereas the highest compressive strength obtained with a confining pressure of 230 MPa is 4.0 GPa. In addition, the compressive strength increased

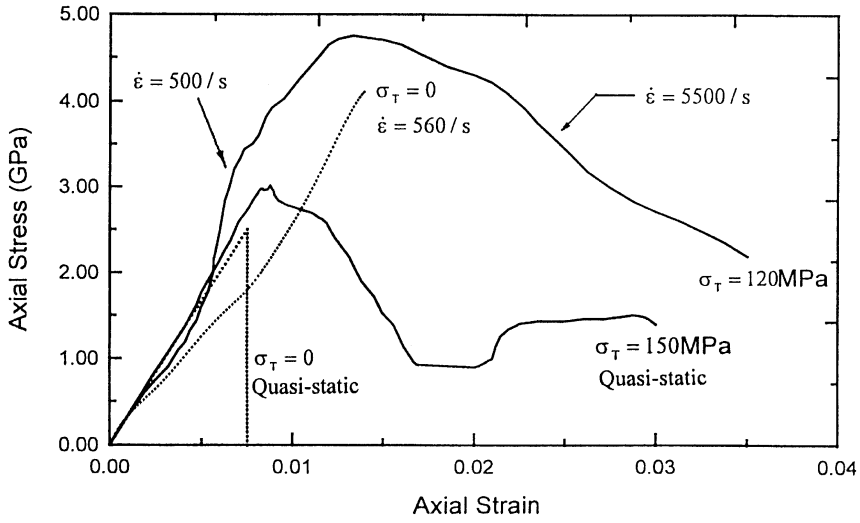

Figure 2. Typical stress-strain response of AlN for unconfined and confined (120 MPa) at a nominal strain rate of $4 \times 10^{-4}\,s^{-1}$ and $5 \times 10^{2}\,s^{-1}$.

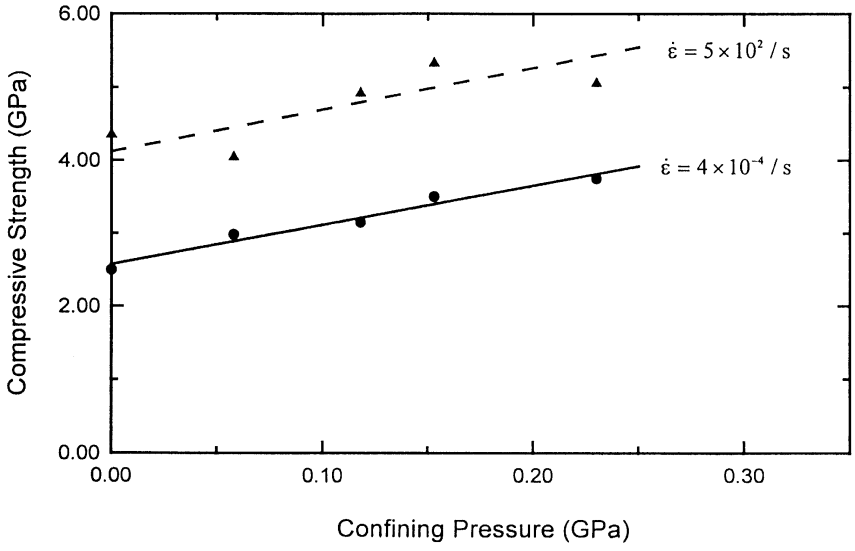

Figure 3. Failure strength of AlN as a function of lateral confinement for nominal strain rates of $4 \times 10^{-4}\,s^{-1}$ and $5 \times 10^{2}\,s^{-1}$.

by approximately 1.5 GPa as the strain rate was increased from 4×10^{-4} to $5 \times 10^{2}\,s^{-1}$, which appeared to be the strain rate effect on the failure strength. The peak or failure strength increases with increase in lateral confinement at both strain rates. Also, the increase in strength at a given lateral confinement between low and high strain rates appears to be constant, i.e., strain rate dependent strength increase appears to be independent of lateral confinement. Results recently obtained by Chhabildas et al. (1997) on sleeved alumina rods indicate that the strength increases with both loading rate and confinement, which are consistent with the present results.

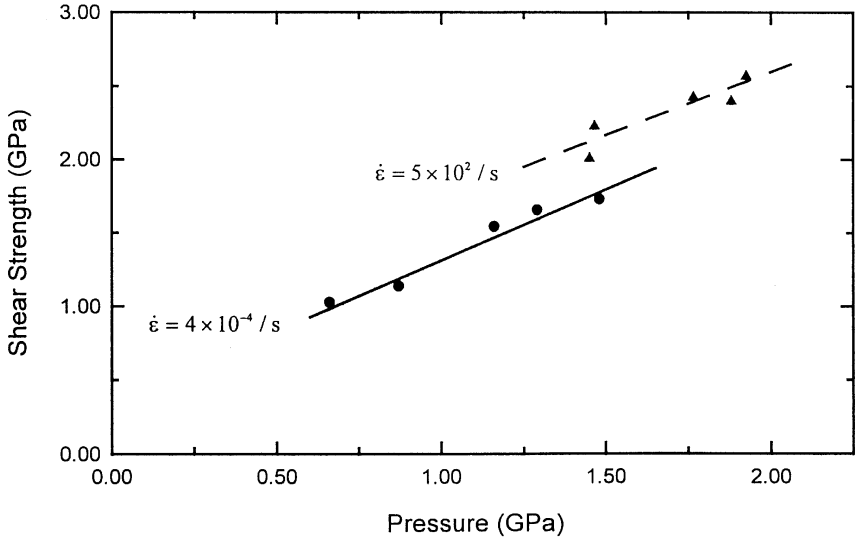

Figure 4. Failure surface for AlN in the pressure-shear strength (p–τ) plane.

3. Failure surface

3.1. Failure criterion for brittle failure

When a brittle solid is loaded by axial compression to failure either quasi-statically or dynamically, theoretical studies indicated that crack initiation, propagation, and interaction are the dominating failure mechanisms; see for example, Horii and Nemat-Nasser (1986), Ashby and Sammis (1990). Figure 4 shows the failure surface on the pressure-shear strength (p–τ) plane of the sintered aluminum nitride (AlN) under dynamic and quasi-static axial compressive loading using the strength data shown in Figure 3 for various levels of lateral confinement.

The results of these theoretical and experimental studies all indicate that the brittle failure behavior of ceramic materials obeys the Mohr–Coulomb failure criterion under either quasi-static or dynamic loading conditions

$$|\tau| + \alpha p = \tau_0, \tag{2}$$

where $|\tau|$ is the absolute value of shear strength, p is the hydrostatic or the hydrodynamic pressure, τ_0 is the shear strength of the material without any pressure (pure shear), and α, referred to as the internal friction coefficient, is the proportionality coefficient between $|\tau|$ and p. As will be demonstrated in the following sections, the simple failure criterion expressed in (2) provides a possible unified approach to interpret experimental results on ceramics obtained by various experimental methods, e.g., Kolsky pressure bar, plate impact and quasi-static compression.

Johnson and Holmquist also provided a failure criterion for brittle materials known as the JH-2 model, see Johnson and Holmquist (1994) and Holmquist et al. (1995) where the normalized strength σ^* is expressed as

$$\sigma^* = \sigma_i^* - D(\sigma_i^* - \sigma_f^*), \tag{3}$$

where σ_i^* is the normalized strength of the intact material, σ_f^* is the normalized strength of the fractured material, and D is the damage parameter ($0 \leqslant D < 1$). The stresses ($\sigma, \sigma_1, \sigma_f$) have been normalized by σ_{HEL}, the equivalent stress at the HEL. The equivalent stress σ_e is defined in terms of principal stresses as

$$\sigma_e = \sqrt{\tfrac{1}{2}[(\sigma_1 - \sigma_2)^2 + (\sigma_2 - \sigma_3)^2 + (\sigma_3 - \sigma_1)^2]}.$$

In the case of a cylindrical specimen subjected to axial and transverse loading, where $\sigma_1 = \sigma$, and $\sigma_2 = \sigma_3 = \sigma_T$, the equivalent stress is simply

$$\sigma_e = \sqrt{\tfrac{3}{2}}(\sigma_A - \sigma_T). \tag{4}$$

The normalized strength of the intact material in the JH-2 model is given by

$$\sigma_i^* = A(P^* + T^*)^N(1 + C \ln \dot{\varepsilon}^*), \tag{5}$$

where A, C and N are material constants to be determined by experiments. The normalized pressure is $P^* = P/P_{\text{HEL}}$, where P is the actual pressure and P_{HEL} is the pressure at HEL. The normalized hydrostatic tension is $T^* = T/P_{\text{HEL}}$, where T is the maximum hydrostatic tension the material can withstand. The actual strain rate $\dot{\varepsilon}$ is normalized by the reference strain rate of $\dot{\varepsilon}_0 = 1.0\,\text{s}^{-1}$ as $\dot{\varepsilon}^* = \dot{\varepsilon}/\dot{\varepsilon}_0$.

The experimental data shown in Figure 4 were used to determine the material constants. First, the damage parameter D is set to be zero ($D = 0$) since the data presented in Figure 4 were obtained from intact sintered AlN specimens (Chen and Ravichandran, 1996b). T can be estimated at the intersection between the failure surface and the p-axis. Then only three material constants need to be determined: A, N, and C. Using the data points in Figure 4 and taking $P_{\text{HEL}} = 4.35\,\text{GPa}$, and $\sigma_{\text{HEL}} = 6.70\,\text{GPa}$ (Grady, 1998), the constants were found to be $A = 1.10$, $N = 0.987$, and $C = 0.0546$. Thus,

$$\sigma_i^* = 1.10(P^* + 0.169)^{0.987}(1 + 0.0546 \log \dot{\varepsilon}^*). \tag{6}$$

Taking the value of N to be approximately 1.0, the above equation for $\dot{\varepsilon} = 500\,\text{s}^{-1}$ can be simplified using the terms of (1) to

$$\tau = 0.93p + 0.62. \tag{7}$$

Comparison of (2) and (7) reveals that they have exactly the same form, with $\alpha = -0.93$ and $\tau_0 = 0.62\,\text{GPa}$. In other words, both the Mohr–Coulomb and the improved Johnson–Holmquist model (JH-2) models appear to converge to the same form when describing the brittle failure behavior of intact ceramic materials.

3.2. Failure criterion for ductile failure

As the pressure further increases beyond the range of Figure 4, the brittle failure mode may be expected to change gradually to ductile failure. Heard and Cline (1980) found in their quasi-static tri-axial experiments that there was a brittle-ductile transition in hot-pressed AlN when confining pressure reached 0.55 GPa. A brittle-ductile transition in failure mode was also

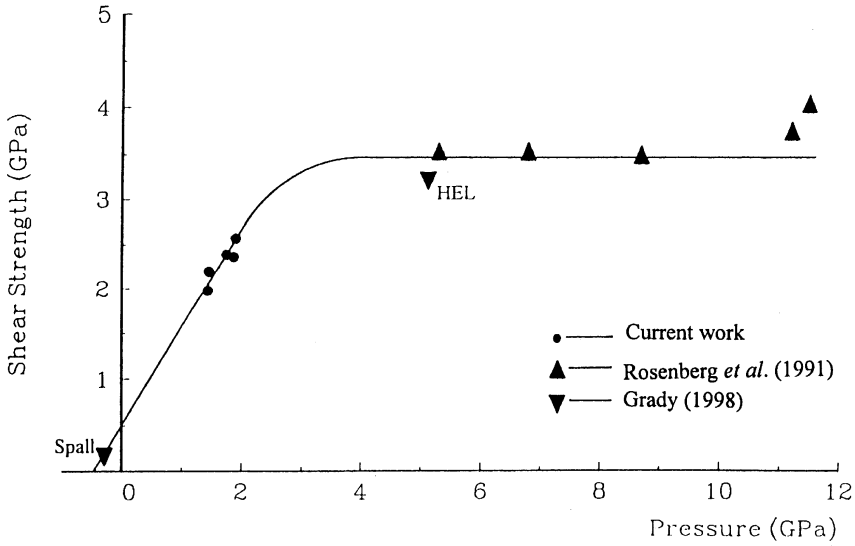

Figure 5. Variation of maximum shear strength of AlN with pressure under dynamic loading conditions.

observed in a glass ceramic, Macor, under dynamic loading conditions (Chen and Ravichandran, 1997). Although a similar transition could not be observed in the dynamic multiaxial experiments on AlN performed by Chen and Ravichandran (1996b) due to the limitations in confinement pressure, the failure surface of AlN shown in Figure 4 may be extended approximately using data from other types of experiments in literature.

The dynamic experimental data in Figure 4 are plotted again in Figure 5, together with the spall strength and Hugoniot elastic limit (HEL) data for AlN reported by Grady (1998). In addition, Rosenberg et al. (1991) also tested AlN at pressure values beyond HEL by using the plate impact technique together with the embedded manganin gage (normal and transverse) technique. Their data are also plotted in Figure 5. Inspection of the results indicates that the shear strength of AlN remains nearly constant at 3.5 GPa after pressure is increased to beyond HEL. Grady's experimental results reported by Dandekar et al. (1994) on the shear strength of AlN in the wurtzite phase also indicated that the shear strength remained nearly a constant, approximately 2.8 GPa at pressure values beyond HEL and up to 18 GPa. The data points at pressures above 11 GPa in Figure 5 indicate that there was an increase in shear strength. This increase was considered by Rosenberg et al. (1991) to be the result of a phase transformation in the material due to the high pressure. Kipp and Grady (1994) have investigated high-pressure phase transformation in AlN under shock wave loading. In our present work, only the failure/flow behavior in AlN under pressures below phase transformation is discussed.

At low confining pressure, the failure surface of AlN appears as a straight line in the p–τ plane as discussed earlier. The inclined straight line is connected by a short convex curve (Figure 5) whose slope decreases continuously as the pressure is increased. This convex curve is constructed to qualitatively represent the transition region between brittle and ductile behavior. The shear strength is essentially constant as the pressure increases from 5 GPa to 11 GPa as shown in Figure 5. The Hugoniot elastic limit is located near the high-pressure end of the brittle-ductile transition region. It should be noted that a straight line parallel to the p-axis in the p–τ plane represents the failure surface of a material that fits a von Mises or Tresca type

of criterion identified with the pressure insensitive plastic flow. This indicates that plastic flow may be the failure mechanism of ceramics under high pressure.

Although the above results focused specifically on the failure surface of AlN in the p–τ plane, the failure criterion may be applicable to other brittle materials. The failure behavior of Al_2O_3, BeO (Heard and Cline, 1980) and granite (Ashby and Sammis, 1990) is very similar to the behavior of aluminum nitride shown in Figure 5. The brittle-ductile transition under quasi-static and dynamic loading conditions have been postulated and analyzed by Horii and Nemat-Nasser (1986) and Deng and Nemat-Nasser (1994). Using a plasticity model based on pressure insensitive shear strength beyond its HEL, Feng et al. (1996) interpreted their shock compression data (axial and lateral stress components measured using embedded manganin gauges) for silicon carbide.

4. Effect of various parameters on the failure surface

4.1. Effect of internal friction

The theoretical analysis (Horii and Nemat-Nasser, 1986; Ashby and Sammis, 1990) on a microscopic sliding crack model shown in Figure 6 using fracture mechanics concluded that a simplified 'wing crack' will start to propagate when

$$\sigma_1 = c\sigma_3 - \sigma_0, \tag{8a}$$

where σ_1 is the axial stress, σ_3 is the transverse stress, c is a material constant which is solely a function of the friction coefficient μ on the sliding crack surfaces

$$c = \frac{(1+\mu^2)^{1/2} + \mu}{(1+\mu^2)^{1/2} - \mu} \tag{8b}$$

and σ_0 is the compressive strength without any lateral confinement which depends on the friction coefficient μ, the fracture toughness $K_{\mathrm{I}c}$, and the pre-existing crack size 'a' in the material

$$\sigma_1 = \frac{(1+\mu^2)^{1/2} + \mu}{(1+\mu^2)^{1/2} - \mu}\sigma_3 - \frac{\sqrt{3}}{(1+\mu^2)^{1/2} - \mu}\frac{K_{\mathrm{I}c}}{\sqrt{\pi a}}. \tag{8c}$$

Equation (8a) is equivalent to the Mohr–Coulomb failure criterion when (assuming $\sigma_2 = \sigma_3$ for axial symmetry or uniaxial strain)

$$p = -\tfrac{1}{3}\sigma_{kk} = -\tfrac{1}{3}(\sigma_1 + 2\sigma_3), \qquad |\tau| = \tfrac{1}{2}|\sigma_1 - \sigma_3|,$$

$$\alpha = \frac{3(c-1)}{2(2+c)}, \quad \text{and} \quad \tau_0 = -\frac{3\sigma_0}{2(2+c)}. \tag{8d, e}$$

The sliding crack model shown in Figure 6 suggests that the shear strength of the material depends on the pressure through friction between the crack surfaces as depicted by the Coulomb law (Jaeger and Cook, 1979). Therefore, the slope of the failure surface line in the brittle failure region of the material depends intrinsically on the friction coefficient of the cracked flaw surfaces. If the stress state at failure of the material is proportional to the stress state

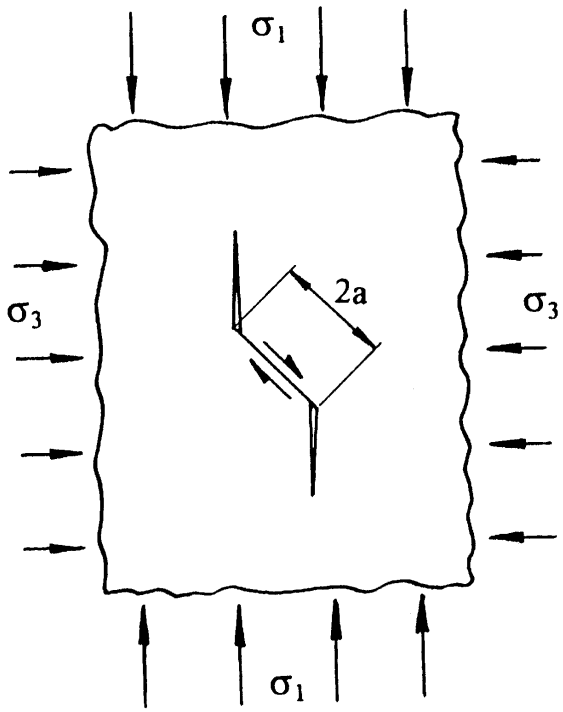

Figure 6. A schematic illustration of a sliding crack model.

at which cracks start to propagate, then the coefficient α in Mohr–Coulomb criterion (2) is related to the coefficient of friction μ by

$$\alpha = -\frac{3\mu}{3(1+\mu^2)^{1/2} - \mu}. \tag{9}$$

The coefficient α is a function of only the friction coefficient, μ, and is not dependent on any of the intrinsic material properties. Figure 7 is a plot of the variation of failure surface slope $-\alpha$ as a function of the friction coefficient μ. The value of $-\alpha$ increases almost linearly as μ increases. When μ reaches a value of 0.8, the rate of the increase in α with increasing μ begins to decrease. For all practical situations, μ must have a value between 0 (free sliding) and ∞ (perfect bonding), and, therefore from (9),

$$-1.5 \leqslant \alpha < 0. \tag{10}$$

When $\alpha = 0$, which represents the free sliding case, the material response will be purely pressure insensitive. A horizontal line in the p–τ plane thus represents the failure surface. As indicated earlier, this matches the description of pressure insensitive plastic flow of ductile materials in the p–τ plane. The case of $\alpha = -1.5$ (no sliding) coincides with the case of uniaxial stress without any lateral confinement in which $p = \frac{1}{3}\sigma$ and $|\tau| = \frac{1}{2}\sigma$, where σ is the applied axial stress. Equation (10) indicates that the value of α for any solid material should be between 0 and -1.5. For AlN, $\alpha = -1$ as determined from Figure 4; the corresponding friction coefficient μ was calculated using (9) to be 1.13. This value is higher than the typical value of the friction coefficient for a brittle material which varies from 0.2 (tungsten carbide

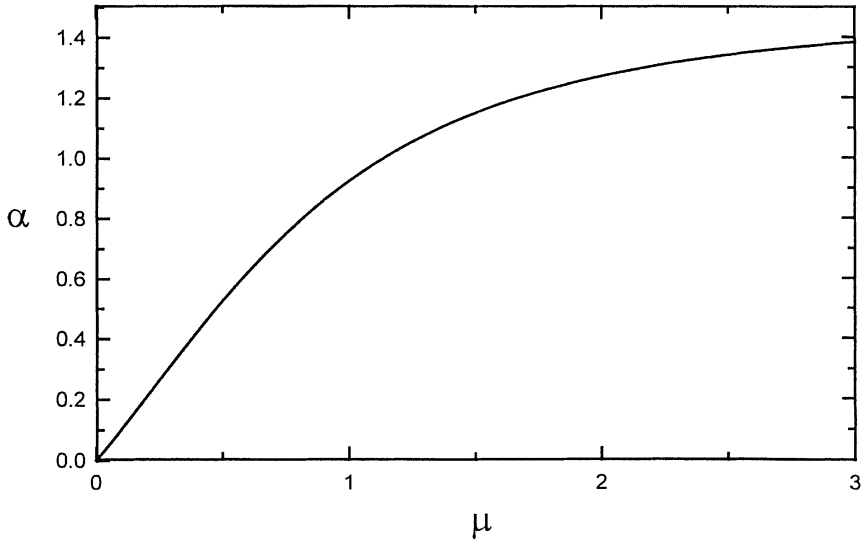

Figure 7. Variation of slope of the failure surface α with friction coefficient μ.

on tungsten carbide) to 0.94 (glass on glass) (Dorf, 1996). There are two possible reasons for this discrepancy. First, the model shown in Figure 6 may be an over simplification of actual failure process, and second, the frictional behavior on the microscale may be different from that measured using two large macroscopically flat surfaces.

4.2. RATE SENSITIVITY OF CERAMICS

As discussed above, the Mohr–Coulomb failure criterion as expressed by (2) describes the failure behavior of a ceramic material when the pressure is below its brittle-ductile transition. The right-hand side of (2) is a pure shear strength term. Ceramics and other brittle materials have been found to be rate sensitive in their uniaxial compressive strengths (e.g., Ravichandran and Chen, 1991; Subhash and Ravichandran, 1998). Under uniaxial stress condition, the axial stress σ may be decomposed into hydrostatic pressure σ_h (p) and deviatoric stress σ_d (τ) as

$$\sigma = \sigma_h + \sigma_d, \tag{11}$$

where $\sigma_h = \sigma/3$ and $\sigma_d = 2\sigma/3$. Under pressures below brittle-ductile transition, the failure mechanisms of brittle materials are mainly crack initiation and propagation as discussed earlier. The effect of hydrostatic pressure is merely to cause the crack closures in the material. Therefore, the rate sensitivity in σ must come from the deviatoric stress σ_d. Similarly, the second term in the left-hand side of the Mohr–Coulomb failure criterion (2) is the hydrostatic pressure term. The rate sensitivity of this term, if any, has to be from the slope of the Mohr–Coulomb failure surface (α) which depends solely on the coefficient of friction (9). The frictional behavior of microcracks is not well understood for brittle materials such as ceramics under dynamic loading conditions. The term in the right-hand side of (2), τ_0, is the deviatoric stress and is expected to be rate sensitive. The strain rate dependence of brittle failure strength has been investigated through thermodynamic energy conditions for spall fracture (Grady, 1988), through statistical crack distributions (Grady and Kipp, 1989), and

through micromechanical modeling of dynamic crack (Ravichandran and Subhash, 1995). All these studies suggest essentially the same strain rate dependence for compressive strength

$$\sigma_f \propto \dot{\varepsilon}^n, \tag{12}$$

where n is around $\frac{1}{3}$ for brittle solids. From the data for AlN (Subhash and Ravichandran, 1998), the rate sensitivity parameter n is found to be around 0.29. The limited data available for AlN (Figure 4) suggests that the rate sensitivity parameter n is unaffected by the magnitude of the confining pressure. This provides some validation for the present hypothesis that the shear strength (τ_0) of the material is rate sensitive. However, the rate dependence of pure shear strength of ceramics is not well understood at the present time and needs further study.

4.3. Effect of damage on failure surface

When undamaged or intact brittle materials are loaded to failure using various experimental techniques, the failure/flow strength data should fall on a failure surface of the type discussed in Section 3. When previously damaged materials are loaded to failure, the operational region under the failure surface is expected to decrease as the extent of the pre-damage is increased. As shown in Figure 8, the pre-damage is characterized by a damage parameter D. The reduction of the operational region has a lower bound set by the complete comminution of the brittle material where no more damage can be introduced, and D assumes its maximum value D_{MAX}. It should be mentioned that the damage parameter couldn't be isotropic even though the brittle material is isotropic before damage occurs. Typically, there are measurable differences in the elastic properties of a recovered brittle specimen along different axes following axial loading by a dynamic pulse of significant enough amplitude to initiate damage. The measured directional dependence of elastic properties of the damaged specimen indicates that the damage parameter D depends heavily on the form of the prior loading and is not isotropic (Subhash and Nemat-Nasser, 1993). At the microscale level, the microstructural change due to material damage depends significantly on the direction of local stress and local strain, and is thereby intrinsically anisotropic (e.g., Murakami, 1987). Therefore, care must be taken in the definition of the damage parameter for brittle materials. However, most existing models are phenomenological and not well connected with the actual process on the microscale (Krajcinovic, 1985). Based on their analytical studies, Krajcinovic and Mastilovic (1995) concluded that the logical choice of damage approximation in a brittle material should be a fourth-order tensor. Therefore, the scalar damage parameter D used in Figure 8 is just a representative to illustrate the effect of damage.

If the failure surface has been reached during the loading process, the material will be either damaged or failed catastrophically. If the material is reloaded after partial or complete unloading during which failure initiated, the further failure behavior of the damaged material will follow the failure surface for damaged material with the corresponding value of D. The shear strength of the damaged material is lower than that of the intact material under the same pressure as depicted in Figure 8. Currently available data for intact AlN described in Section 3.2 is included in Figure 8. The quantitative relation between the damage parameter and the damage surface for ceramics remains to be explored.

When the damage reaches the maximum, the ceramic material is completely comminuted. The high strain rate behavior under confining pressure of granulated ceramics have been investigated by Klopp and Shockey (1991) and Sairam and Clifton (1994) using the pressure-shear

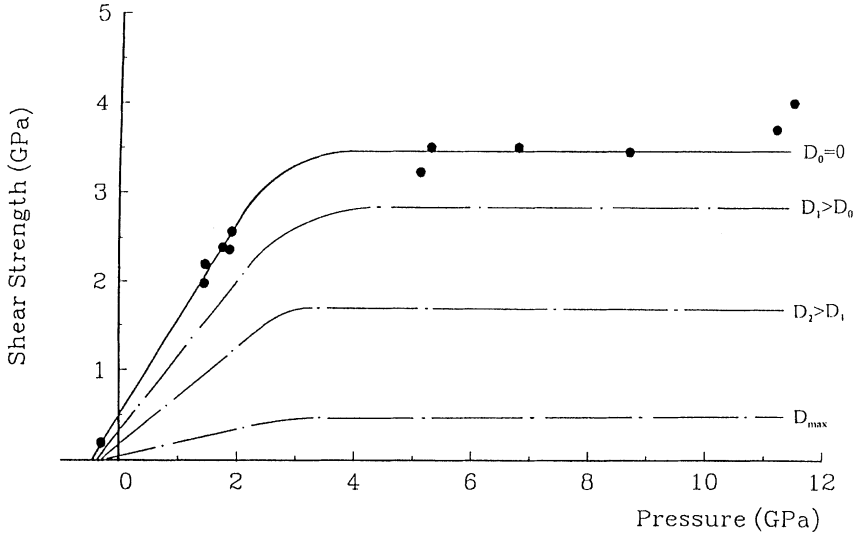

Figure 8. Illustration of the effect of damage on the failure surface for brittle materials.

plate impact technique. Their results show that in this limiting state, the ceramic powders behave like a Mohr–Coulomb materials with a slope (i.e., the α in (2)) of approximately 0.2.

4.4. Effect of Poisson's Ratio on Failure Behavior

If the stress state is uniaxial strain in an experiment below the HEL, the lateral stress σ_T induced by the axial stress σ is proportional to the axial stress through the Poisson's ratio ν

$$\frac{\sigma_T}{\sigma} = \frac{\nu}{1-\nu}. \tag{13}$$

It is clear that for small values of ν, the values of σ_T/σ are also small. Therefore the lateral stress induced by a given axial load is relatively small. In an experiment of dynamic uniaxial strain stress state, e.g., a shock compression experiment, the material with low Poisson's ratio is expected to initiate the failure process by axial splitting because the lateral confining pressure is not sufficient to completely suppress the tendency for crack initiation and propagation. Therefore, ceramic materials with low Poisson's ratios would tend to fail by brittle cracking that leads to fragmentation. On the other hand, a higher Poisson's ratio will induce higher confinement under axial compression as depicted by (13) under uniaxial strain condition. The large lateral confinement prevents the microcracks from sliding and brittle failure. Thus the associated failure mode may be expected to change from complete brittle failure with low values of ν, to pressure insensitive plastic flow with large values of ν. This suggests that the value of the Poisson's ratio of a material may indicate the degree of the brittleness of the material at least under conditions of plane strain. Similar arguments based on (8c) have been used by Wright and Ravichandran (1996) to explain the observed behavior in spall strengths in TiB_2 ($\nu = 0.05$) and Al_2O_3 ($\nu = 0.24$). Recently, Bhattacharya et al. (1998) have proposed an analytical model to explain the experimentally observed strength dependence of ceramics on lateral confinement and Poisson's ratio. It is also interesting to note that most ceramics have a Poisson's ratio between 0 and 0.25 (Table 2) and most metals have a Poisson's ratio higher than 0.25 but less than 0.5.

4.5. BRITTLE VERSUS DUCTILE RESPONSE AT HIGH PRESSURES

It is interesting to note that elasticity theory also suggests an increase in theoretical yield strength with the decrease in Poisson's ratio. The shear modulus G can be expressed in terms of Young's modulus E and Poisson's ratio ν

$$G = \frac{E}{2(1+\nu)}. \tag{14}$$

The shear strength τ_y of a material is a fraction of the shear modulus G, i.e.,

$$\tau_y = \frac{G}{M} = \frac{E}{2M(1+\nu)}, \tag{15}$$

where M is a constant whose value is in the order of 30–1,000 for most engineering materials. It is clear from the inspection of (15) that the materials with higher Poisson's ratio values will have lower shear strengths, indicating that plastic deformation may be activated if Schmid (Schmid and Boas, 1935) law for flow on favorably oriented slip systems is satisfied. On the other hand, if the Poisson's ratio of a material is low, the shear strength will be relatively high. In this case, the material will fail by cracking before the critical resolved shear stress for flow is reached even under uniaxial strain condition in experiments such as plate impact loading.

Besides Poisson's ratio, spall strength is also an indicator of the brittleness of a material. Small spall strength indicates that the material is very brittle in tension, and the tensile strength is dominated by the propagation of a single dominant flaw in the material. On the other hand, a large spall strength, which implies a high fracture toughness, indicates that the propagation of the crack may not be brittle even though the material itself maybe categorized as brittle such as WC and ZrO_2 (Grady, 1998).

Horii and Nemat-Nasser (1986) proposed another parameter referred to as ductility Δ as an indication of material failure behavior in terms of the degree of brittleness under quasi-static loading conditions. The ductility was defined as

$$\Delta = \frac{K_{\mathrm{I}c}}{\tau_y(\pi a)^{1/2}}, \tag{16}$$

where τ_y is the shear strength of the material, and 'a' is the half length of the pre-existing crack shown in Figure 6. A microcrack starts to grow under local tensile stress when the stress intensity reaches its critical value, $K_I = K_{\mathrm{I}c}$. The higher the value of Δ, the more ductile the material.

Under dynamic loading conditions, the fracture toughness can be calculated from the surface energy which can be measured in the spall experiments. The shear stress at HEL, τ_{HEL} may be taken as yield strength, τ_y. From fracture mechanics, the fracture toughness is converted from surface energy Γ using the formula

$$K_{\mathrm{I}c} = \begin{cases} \sqrt{2E\Gamma} & \text{for } 1-D \text{ stress}, \\ \sqrt{\dfrac{2E\Gamma}{1-\nu^2}} & \text{for } 1-D \text{ strain}, \end{cases} \tag{17}$$

where E is the Young's modulus and ν is the Poisson's ratio of the material. Grady (1998) reported Γ and HEL data for a variety of ceramic materials. Table 2 lists the values of the

Table 2. Parameters for ceramics describing their ductility.

Material	E^* GPa	ν^*	Γ^* J/m^2	K_{Ic} MPa m$^{1/2}$	τ^*_{HEL} GPa	Δ	σ_0 GPa	Λ
TiB_2	523	0.05	27	5.3	7.34	0.23	1.8[a]	0.25
SiO_2	90	0.08	9.5	1.3	3.65	0.12	2.0[b]	0.54
SiC	434	0.16	12	3.2	6.27	0.17	2.75[b]	0.42
B_4C	462	0.17	31.5	5.4	7.16	0.24	2.4[b]	0.32
WC	627	0.21	668	28.9	1.84	5.11	5.3[b]	1.91
AlN	321	0.24	38	4.9	2.74	0.58	2.5[c]	0.91
Al_2O_3	401	0.24	38	5.5	3.93	0.46	2.07[d]	0.47
ZrO_2	218	0.31	970	20.6	3.99	1.68	2.84[e]	0.57

*Grady (1998), [a]Meyers et al. (1991); [b]Goodfellow Ceramic Data Table (1992); [c]Present study, Table 1; [d]Coors Ceramics Company Data Sheet (1991); [e]Richerson (1992).

'ductility' for ceramics calculated from Grady's data. The flaw size is taken to be $a = 3\,\mu$m in the calculations, which is a typical average grain size of many modern engineering ceramics.

Since $K_{Ic} \propto \sigma_0\sqrt{\pi a}$ (see (8c) where σ_0 is the uniaxial (unconfined) *quasi-static* compressive failure strength of the material, a new nondimensional ductility parameter Λ may be introduced

$$\Lambda = \frac{\sigma_0}{\tau_{HEL}} \tag{18}$$

and appears to be equivalent to the ductility parameter Δ defined in (16). However, the parameter Λ is much easier to be experimentally determined, since σ_0 is relatively easier to measure than K_{Ic}. Furthermore, the flaw size 'a' is not involved in computing Λ. The values of Λ for various engineering ceramics are also listed in Table 2.

Since the values of σ_0 listed in Table 2 are collected from a variety of sources (e.g., Meyers et al., 1991; Richerson, 1992; Subhash and Ravichandran, 1998), they may not exactly correspond to the materials used by Grady (1998). Therefore, the values of Λ listed in Table 2 should be considered to reflect its trend or qualitative nature. However, as listed in Table 2, both ductility parameters Δ and Λ show that WC and ZrO_2 are the most 'ductile' ceramics listed in the Table 2, followed by AlN and Al_2O_3.

5. Limitations of the failure/flow surface

The validity of the failure/flow failure surface proposed in this paper provides a possible unified framework under which the experimental results on ceramic materials obtained using various experimental techniques may be properly interpreted in the p–τ plane. However, the limitations on the applicability of the model should be thoroughly understood. Careful inspection of the construction of the failure surface indicates that attention should be paid to the following aspects when applying the failure surface.

5.1. Existence of the failure surface

Stable crack propagation under quasi-static compressive loading may ensure the existence of a compressive failure criterion, since a population of small cracks extends in a stable manner under compression. Each of the cracks grows longer as the stress is raised, until they interact in some cooperative way to give final failure (Ashby and Sammis, 1990). In the case of dynamic loading conditions, the stability of dynamic crack propagation under overall compressive loading needs to be studied. The failure surface may exist only when the dynamic microcrack propagation is stable under compressive loading, such that the cracks will stop propagating when the load level is not increasing.

5.2. Appropriate choice of the failure surface

It was pointed out earlier that the failure surface constructed from the available experimental data is applicable only for undamaged or intact materials because the strength data were obtained for the intact materials. For damaged materials, a damage parameter, which will not be isotropic as described earlier, should be properly defined. A series of failure surfaces characterized by the damage parameter can then be constructed based on the extent of damage. These failure surfaces for materials in damaged states are important in accurately representing the post-failure behavior of the material. It is interesting to note that after being loaded to a sufficiently high level, ceramics will be comminuted upon load reversal, which indicates that the material properties have been altered dramatically by the load-induced damage. On the other hand, upon load reversal, the flow behavior of ductile materials will be affected only by the Bauschinger effect. The failure modes in ceramics are widely varied, ranging from perfectly brittle failure induced by a single crack to possibly total communition under hydrostatic loading conditions. The choice of failure envelopes and their relation to the range of failure modes remains to be understood.

6. Summary and conclusions

- An experimental technique capable of applying dynamic axial compression with lateral confinement on a cylindrical ceramic specimen has been developed. During the experiment, the specimen is subjected to a single, well-defined loading pulse which enables the recovery of ceramic specimens for deformation and failure mode characterization.
- Based on the experimental results on AlN together with available data in literature, a failure/flow surface is constructed for ceramics under high pressure loading. This model provides a possible unified framework under which the experimental results on ceramic materials from various experimental techniques may be properly interpreted and compared. Mohr–Coulomb criterion and improved Johnson–Holmquist model were found to fit the experimental data for brittle failure at low pressures, whereas the materials deformed in a manner similar to pressure insensitive plastic flow at high pressures.
- Influence of damage on the proposed failure surface for ceramic materials has been qualitatively described. Damage in general degrades the shear strength of ceramic materials.
- The Poisson's ratio of a ceramic material plays an important role in influencing failure modes observed in the material especially under conditions of uniaxial or plane strain. Experimental observation based on shock wave studies of ceramic could be explained in terms of the lateral confinement due to Poisson's ratio effect.

Acknowledgments

The authors acknowledge the support of the Army Research Office (DAALO3-02-G-0192), the National Science Foundation (CMS-9157846) and the Dow Chemical Company for this research. Many helpful discussions with Dr. D.E. Grady are gratefully acknowledged.

References

Ashby, M.F. and Sammis, C.G. (1990). The damage mechanics of brittle solids in compression. *PAGEOPH* **133**, 489–521.

Bhattacharya, K., Ortiz, M. and Ravichandran, G. (1998). Energy-based model of compressive splitting in heterogeneous brittle solids. *Journal of the Mechanics and Physics and Solids* **46**, 2171–2181.

Chhabildas, L.C., Furnish, M.D. and Grady, D.E. (1997). Impact of alumina rods – A computational and experimental study. *Journal de Physique* **7(C3)**, 137–143.

Chen, W. and Ravichandran, G. (1996a). An experimental technique for imposing dynamic multiaxial-compression with mechanical confinement. *Experimental Mechanics* **36**, 435–438.

Chen, W. and Ravichandran, G. (1996b). Static and dynamic compressive behavior of aluminum nitride under moderate confinement. *Journal of American Ceramic Society* **79**, 579–584.

Chen, W. and Ravichandran, G. (1997). Dynamic compressive failure of a glass ceramic under lateral confinement. *Journal of the Mechanics and Physics of Solids* **45**, 1303–1328.

Chen, W., Subhash, G. and Ravichandran, G. (1994). Evaluation of ceramic specimen geometries used in a split Hopkinson pressure bar. *Dymat Journal* **1**, 193–210.

Dandekar, D.P., Abbate, A. and Frankel, J. (1994). Equation of state of aluminum nitride and its shock response. *Journal of Applied Physics* **76**, 4077–4085.

Deng, H. and Nemat-Nasser, S. (1994). Dynamic damage evolution of solids in compression – microcracking, plastic-flow, and brittle-ductile transition. *Journal of Engineering Materials* **116**, 286–289.

Dorf, R.C. (1996). *The Engineering Handbook*, CRC Press.

Feng, R., Raiser, G.F. and Gupta, Y.M. (1996). Shock response of polycrystalline silicon-carbide undergoing inelastic deformation. *Journal of Applied Physics* **79**, 1378–1387.

Follansbee, P. (1985). The Hopkinson bar, in Mechanical Testing, Metals Handbook, Vol. 8 [9th ed.], pp. 198–217, American Society for Metals, Metals Park, Ohio.

Grady, D.E. (1988). The spall strength of condensed matter. *Journal of the Mechanics and Physics of Solids* **36**, 353–383.

Grady, D.E. and Kipp, M.E. (1989). Fragmentation of solids under dynamic loading, (Edited by T. Wurzbicki). *Structural Failure* pp. 1–39, John Wiley and Sons.

Grady, D.E. (1998). Shock wave compression of brittle solids, in *Mechanics of Materials* in press.

Heard, H.C. and Cline, C.F. (1980). Mechanical behavior of polycrystalline BeO, Al_2O_3 and AlN at high pressure. *Journal of Materials Science* **15**, 1889–1897.

Holmquist, T.J., Johnson, G.R., Grady, D.E., Lopatin, C.M. and E.S. Hertel, Jr. (1995). High strain rate properties and constitutive modeling of glass, in: *Proceedings of the 15th International Symposium on Ballistics*, Jerusalem, Israel, May 21–24.

Horii, H. and Nemat-Nasser, S. (1986). Brittle failure in compression: splitting, faulting and brittle-ductile transition. *Philosophical Transaction of the Royal Society of London* **A319**, 337–374.

Jaeger, J.C. and Cook, N.G.W. (1979). *Fundamentals of Rock Mechanics*, Chapman and Hall.

Johnson, G.R. and Holmquist, T.J. (1994). An improved computational model for brittle materials, (Edited by S.C. Schmidt, J.W. Shaner, G.A. Samara and M. Ross). *High Pressure Science and Technology – 1993*, American Institute of Physics.

Kipp, M.E. and Grady, D.E. (1994). Shock phase transformation and release properties of aluminum nitride. *Journal de Physique IV* **4(C8)**, 249–256.

Klopp, R.W. and Shockey, D.A. (1991). The strength behavior of granulated silicon carbide at high strain rate and confining pressure. *Journal of Applied Physics* **70**, 7318–7326.

Kolsky, H. (1949). An investigation of the mechanical properties of materials at very high rates of loading. *Proceedings of the Royal Society of London* **B62**, 676–700.

Krajcinovic, D. (1985). Constitutive theories for solids with defective microstructure, (Edited by N. Stubbs and D. Krajcinovic). *Damage Mechanics and Continuum Modeling*, ASCE, New York, 39–56.

Krajcinovic, D. and Mastilovic, S. (1995). Some fundamental issues of damage mechanics. *Mechanics of Materials* **21**, 217–230.

Lankford, J. (1977). Compressive strength and microplasticity in polycrystalline alumina. *Journal of Materials Science* **12**, 791–796.

Lankford, J. (1994). Utilization of the split Hopkinson pressure bar under hydrostatic confining pressure to characterize the compressive behavior of ceramics and ceramic composites, (Edited by A. Gilat). *Mechanical Testing of Ceramics and Ceramic Composites*, AMD 197, ASME, New York, 1–12.

Meyers, M.A., Lasalvia, J.C., Meyer, L.W., Hoke, D. and Niiler, A. (1991). Reaction synthesis dynamic compaction of titanium carbide and titanium diboride. *Journal de Physique III* **1(C3)**, 123–130.

Murakami, S. (1987). Anisotropic aspects of material damage and application of continuum damage mechanics, (Edited by D. Krajcinovic and J. Lemaitre) *Continuum Damage Mechanics, Theory and Applications*, Springer-Verlag, Wien-New York, 91–133.

Murrel, S.A.F. (1963). A criterion for brittle fracture of rocks and concrete under tri-axial stress and the effect of pore pressure on the criterion, (Edited by C. Fairhurst). *Rock Mechanics*, Pergaman, Oxford.

Rajendran, A.M. (1994). Modeling the impact behavior of AD85 ceramic under multiaxial loading. *International Journal of Impact Engineering* **15**, 749–768.

Ravichandran, G. and Chen, W. (1991). Dynamic failure of brittle materials under uniaxial compression, (Edited by K.-S. Kim). *Experiments in Micromechanics of Fracture Resistant Materials*, pp. 85–90. AMD-Vol. 130, ASME, New York.

Ravichandran, G. and Subhash, G. (1995). A micromechanical model for high strain rate behavior of ceramics. *International Journal of Solids Structures* **32**, 2627–2646.

Richerson, D.A. (1992). *Modern Ceramic Engineering*, 2nd edition, Marcel Dekker, Inc., New York.

Rosenberg, Z. (1993). On the relation between the Hugoniot elastic limit and the yield strength of brittle materials. *Journal of Applied Physics* **74**, 752–753.

Rosenberg, Z., Brar, N.S. and Bless, S.J. (1991). Dynamic high-pressure properties of AlN ceramic as determined by flyer plate impact. *Journal of Applied Physics* **70**, 167–169.

Sairam, S. and Clifton, R.J. (1994). Pressure-shear impact investigation of dynamic fragmentation and flow of ceramics, (Edited by A. Gilat). *Mechanical Testing of Ceramics and Ceramic Composites*, AMD 197, ASME, New York.

Schmid, E. and Boas, W. (1935). *Kristallplastizitat*, Springer-Verlag, Berlin.

Subhash, G. and Nemat-Nasser, S. (1993). Dynamic stress induced transformation and fracture formation of Zirconia ceramics. *Journal of American Ceramic Society* **76**, 153–165.

Subhash, G. and Ravichandran, G. (1998). Mechanical behavior of a hot pressed aluminum nitride under uniaxial compression. *Journal of Materials Science* **33**, 1933–1939.

Wright, T.W. and Ravichandran, G. (1996). On shock induced damage in ceramics. *Contemporary Research in the Mechanics and Mathematics of Materials*, (Edited by R.C. Batra and M.E. Beatty), CIMNE, Barcelona, Spain, 480–488.